SANDIA REPORT

SAND2012-7381
Unlimited Release
Printed August 2012

Titanium Subhydride Potassium Perchlorate ($TiH_{1.65}/KClO_4$) Burn Rates from Hybrid Closed Bomb-Strand Burner Experiments

Marcia A. Cooper
Michael S. Oliver

Prepared by
Sandia National Laboratories
Albuquerque, New Mexico 87185 and Livermore, California 94550

Sandia National Laboratories is a multi-program laboratory managed and operated by Sandia Corporation, a wholly owned subsidiary of Lockheed Martin Corporation, for the U.S. Department of Energy's National Nuclear Security Administration under contract DE-AC04-94AL85000.

Sandia National Laboratories

Issued by Sandia National Laboratories, operated for the United States Department of Energy by Sandia Corporation.

Available to DOE and DOE contractors from
U.S. Department of Energy
Office of Scientific and Technical Information
P.O. Box 62
Oak Ridge, TN 37831

Telephone:	(865) 576-8401
Facsimile:	(865) 576-5728
E-Mail:	reports@adonis.osti.gov
Online ordering:	http://www.osti.gov/bridge

Available to the public from
U.S. Department of Commerce
National Technical Information Service
5285 Port Royal Rd
Springfield, VA 22161

Telephone:	(800) 553-6847
Facsimile:	(703) 605-6900
E-Mail:	orders@ntis.fedworld.gov
Online ordering:	http://www.ntis.gov/help/ordermethods.asp?loc=7-4-0#online

SAND2012-7381
Unlimited Release
Printed August 2012

Titanium Subhydride Potassium Perchlorate ($TiH_{1.65}$/$KClO_4$) Burn Rates from Hybrid Closed Bomb-Strand Burner Experiments

Marcia A. Cooper and Michael S. Oliver
Explosives Technologies Group
Sandia National Laboratories
P.O. Box 5800, MS 1454
Albuquerque, NM 87185-1454
macoope@sandia.gov

Abstract

A hybrid closed bomb-strand burner is used to measure the burning behavior of the titanium subhydride potassium perchlorate pyrotechnic with an equivalent hydrogen concentration of 1.65. This experimental facility allows for simultaneous measurement of the closed bomb pressure rise and pyrotechnic burn rate as detected by electrical break wires over a range of pressures. Strands were formed by pressing the pyrotechnic powders to bulk densities between 60% and 90% theoretical maximum density. The burn rate dependance on initial density and vessel pressure are measured. At all initial strand densities, the burn is observed to transition from conductive to convective burning within the strand. The measured vessel pressure history is further analyzed following the closed bomb analysis methods developed for solid propellants.

Contents

Figures

Tables

1 Introduction

Devices containing pyrotechnic powders are utilized in a wide range of defense and commercial applications ranging from nuclear weapon components to automobile airbags to firework displays for their ability to rapidly generate high gas pressures suitable for performing mechanical work. Pyrotechnics rapidly generate gas from chemical reactions that occur within a burn front propagating through the material. The rate of mass consumption of the pyrotechnic into gaseous products within this moving burn front depends on the intrinsic burning rate r of the material and the burning surface area. The intrinsic burning rate is primarily determined by the chemical ingredients, their proportions in the composition and their thermochemical properties. Non-ideal processes associated with phase changes, chemical impurities, and macroscopic properties may alter the combustion characteristics, or intrinsic burning rate, causing variations in performance (Kosanke *et al.*, 2004). As with many other energetic materials, the intrinsic burning rate is typically described with a steady state burning rate law. The formalism often used is that of Vieille's equation, $r = a_0 + a_1 P^n$, where a_1 and n are empirically fitted to closed bomb and/or strand burner data over specified pressure ranges and a_0 is taken as zero. If the initial burning surface area linearly progresses, as in the case of conductive burning, the intrinsic burning rate also represents the surface regression rate. Thus, the mass regression rate dm/dt can be calculated from the condensed phase density, burning surface area and surface regression rate. This is commonly followed for the case of solid propellants, where the intrinsic burning rate of the propellant can be directly related to the linear regression distance with consideration of the burning surface area as determined from the propellant grain geometry (viz. slab, cord, single- or multi-perforated grain) (AMC, 1964).

As one could expect however, such calculations are not nearly as simple for pyrotechnics which are generally used in devices as pressed powder beds containing connected porosity, locally-varying density gradients, and no added binder. The gas pressures generated from the moving burn front may cause events such as powder grain or powder bed fragmentation, powder bed compaction, flame acceleration into powder bed cracks or connected porosity, or distortion of the particle surface area by phase changes. Each of these effects result in changes to the burning surface area invalidating the assumption of linear regression rate (Velicky, 1983; Tao *et al.*, 1989). Because of these complications, computational prediction of the burn rates in pyrotechnics is still a significant challenge such that most system-level performance predictions must rely on historically-used empirical relations that assume a linear burning surface area regression which may not even be remotely applicable for porous pyrotechnic beds in certain situations. As our needs for computational predictive capabilities grow to include the assessment of performance margins, off-normal operation, and changing material characteristics such as manufacturing lot variations, the models derived by empirically fitting experimental data with a single relationship will need to be replaced with a science-based model that captures the critical physics. For the case of combustion in pressed powder beds of pyrotechnics, this includes the ability to predict the burning surface area in porous beds by addressing bed compaction, in-pore combustion, and multiphase flow of the combustion gases and condensed phase particles. This is an incredibly complicated problem that will require advanced computional algorithms in addition to more precise, highly-diagnosed experimental data. We only begin to address these needs by collecting data from the titanium subhydride potassium perchlorate pyrotechnic ($TiH_{1.65}/KClO_4$ or THKP) in an experimental facility that is well-characterized experimentally and analytically in the literature for solid propellant studies.

Historically, titanium potassium perchlorate ($Ti/KClO_4$) (Massis, 1996) and titanium hydride potassium perchlorate ($TiH_2/KClO_4$) (Sorensen *et al.*, 2006; Massis *et al.*, 1975) have been extensively studied. More recently, titanium subhydrides (TiH_x) with equivalent hydrogen concentrations of 0.45 < x <1.9 have been used in more applications (Massis, 1996; Collins *et al.*, 1980). During the late 1980's and coinciding with the powder characterization activities on these subhydrides (Erickson *et al.*, 1986, 1989; Erickson, 1984; Rogers, Jr. *et al.*, 8 89; Begeal and Stanton, 1982; Baer and Shepherd, 1983), the majority of the burn rate studies on $TiH_x/KClO_4$ were carried out by two sets of researchers.

Beginning in 1986, the first measurements on the combustion behavior of $TiH_x/KClO_4$ for values of 0.65 < x < 1.2 were conducted in a closed vessel using single-pellet pyrotechnic strands (Holy, 1986). The collected data consists of the burn time and the pressure-time behavior within the vessel. Because a single pellet is tested, the pressure rise within the vessel is modest and the experiment approximates the isobaric strand burner method with the added pressure-time diagnostic. The pressure data was used to deduce the burning time duration, extrapolate a linear surface regression rate, and measure deviations from this constant rate. Multiple experiments, conducted over a range of initial pressures within the vessel, established the dependence of the surface regression rate on pressure. The steady state burning rate law was fit to the data in which a linear surface regression rate was assumed, thus ignoring the effects of an increased burning surface area in derivation of the rate law. More recently (Holy, 1993), the same methods were applied to $TiH_2/KClO_4$/Viton mixtures allowing for comparisons to be made with the earlier work on $TiH_x/KClO_4$ and conclusions to be drawn about the effect of the Viton additive on the conductive-to-convective burning transition.

Also in the late 1980's, an experimental (Hingorani-Norenberg and Moore, 1987; Hingorani-Norenberg *et al.*, 1990) and modeling (Razani and Shahinpoor, 1988; Razani *et al.*, 1990b,a) effort at SNL/NM was aimed at understanding the zero-free-volume closed bomb burn behavior of $TiH_{1.65}/KClO_4$. These experiments observed dynamics of the accelerating combustion front and the corresponding bed compaction processes resulting from the rapid increase in bomb pressure. Capturing enough data to determine trends in the zero-free-volume case was found to be incredibly challenging due to the extremely high pressures generated and strength limitations of the confinement vessels. Early models of conductive burning behavior by Razani and Shahinpoor initially studied the problem analytically using the ideal gas equation of state, but later transitioned to modifying TIGER for increased complexity enabling the use of other equations of state. Noting that much of the gas phase data is missing in the literature for the combustion products, many parameters were estimated. Comparison of the model results to the limited experimental data was generally not possible.

In this work, we focus on the subhydride with an equivalenct hydrogen concentration of

1.65. To augment the available burn rate data of $TiH_{1.65}/KClO_4$ in the literature, experiments were conducted in a hybrid closed bomb-strand burner using pyrotechnic strands with bulk densities between 60% and 90% theoretical maximum density (TMD). We are able to leverage the data analysis techniques and analytical representations abundant in the literature for solid propellant strand burner measurements for application to these pyrotechnic studies. The tested pyrotechnic strands have a length-to-diameter ratio of six suitable for acquiring additional information about the conductive to convective burn transition. The next sections provide details of the strand burner setup, strand assembly, data analysis and comparison to the literature.

2 Experimental

2.1 Pyrotechnic Material

The $TiH_{1.65}/KClO_4$ material was produced as described in Massis (1996). The ambient pressure crystalline density of THKP is ρ_c =2.84 g/cc which is calculated from the mixture of $TiH_{1.65}$ and $KClO_4$ which have crystalline densities of 3.82 and 2.524 g/cc respectively. The powder was pressed into pellets with nominal densities between 58% and 88% TMD using one of two hydraulic presses used for energetic materials (Carver Monarch CMG30-15-BLP or OTC/SPX Model 1834). Nominal measurements of the pellet dimensions and masses given in Table 1.

$\phi = \rho/\rho_c$ (%TMD)	Density, ρ (g/cc)	Mass (g)	Diameter (in)	Height (in)
58.12±0.55	1.6507±0.0156	0.3367±0.0033	0.2511±0.0006	0.2513±0.0006
67.84±0.28	1.9268±0.0079	0.3990±0.0008	0.2527±0.0004	0.2520±0.0002
79.94±0.22	2.2702±0.0063	0.4623±0.0005	0.2513±0.0003	0.2507±0.0004
88.29±0.51	2.5075±0.0144	0.5202±0.0025	0.2527±0.0002	0.2525±0.0009

Table 1. Details of pyrotechnic pellets of different average densities.

2.2 Strand Assembly

Six pyrotechnic pellets were stacked to from a single strand with two black powder initiating pellets on one end. Two 36 AWG nickel chromium (NiCr) ignitor wires were placed between the two black powder pellets, each 0.635 cm (0.25 inch) in diameter and 0.30 cm (0.117 inch) tall. Combustion of the black power pellets was assumed to uniformly ignite the neighboring pyrotechnic pellet. Breakwires were located between the second black powder pellet and the first pyrotechnic pellet and between subsequent neighboring pyrotechnic pellets for a total of six breakwires equally spaced at 6.35 mm (0.25 inch). The strand was installed within a Delrin® support fixture that contained metal contacts for electrical connection of the break wires and ignition wire as shown in Fig. 1. The support assembly had nominal dimensions of 12.7 cm (5 inches) tall and 3.5 cm (1.4 inches) diameter. The pressure rise in the chamber due to the ignition increment pellets was nominally 0.15 psi as determined from the arrival time of the combustion front at the first break wire.

The breakwires were short pieces of 99.9% pure silver wire with a diameter of 78.48 microns (0.0031 inch). Due to the rigidity of the pellets, locating the break wires in between the pellets resulted in a small gap to exist over the cross section. This resulted in recording "blips" in the pressure data and visual observation of a disturbance to the propagating burn

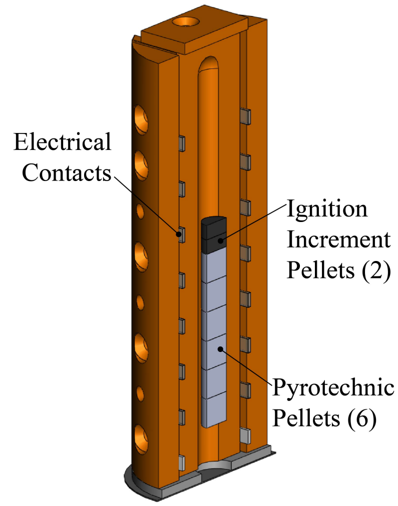

Figure 1. Illustration of test sample consisting of six pyrotechnic pellets, two ignition increment pellets, and the strand support assembly.

front in a bench-top, ambient experiments. In later tests, the top surface of each pellet was scribed creating a trough for the breakwire thus eliminating any gaps at the interface between neighboring pyrotechnic pellets. Due to the small diameter of the silver wire and relatively low melting temperature of silver, it is assumed that the diagnostic wires break at early time when first coming into contact with the propagating burn front. The uniform recess of each wire below the top surface of each neighboring pellet does not affect the burn rate determination. When installed within the reaction vessel, the break wires complete a circuit. Analysis of the circuit resistances and resistance at the connections confirm that the wires are considered broken when the recorded signal first deviates from the baseline. Additional voltages are recorded in the signals but this is assumed to be due to residual metal in the vessel (i.e., titanium) and unconfined, broken wires contacting other electrically conductive surfaces.

During assembly of the strand, a Teflon fixture facilitated pellet alignment while applying a slight longitudinal force to reduce any gaps between the pellets due to placement of the breakwire. Short sections of fiberglass sheathing are then slid over the breakwires to protect them from failure outside the strand. The strand is then coated with one layer of Barco Bond, MB-185 five-minute epoxy gluing the pellets to one another and the fiberglass sheathing to the strand. This epoxy layer was estimated to have a nominal thickness of 1 mm. After the Barco Bond epoxy cured, the strand was easily removed from the Teflon fixture. At this point two more layers of Hardman Adhesives Extra-Fast Setting Epoxy was painted onto the layer of Barco Bond.

2.3 Hybrid Closed Bomb-Strand Burner Description

Our hybrid closed bomb-strand burner, manufactured by Fluitron, Inc., is illustrated in Fig. 2. The experimental facility consists of the main vessel which contains the test sample, a support structure and gas handling system suitable for experimental pressures up to 345 MPa (50 ksi). The main vessel is a cylinder nominally 40.64 cm (16 inches) long with an outer diameter of 21.6 cm (8.5 inches) and an inner diameter of 3.81 cm (1.5 inches). The vessel is sealed with threaded plugs at the top and bottom. The top vessel plug contains feedthroughs for the internal electrical connections, internal mounts for the strand support assembly, and plumbing connections for the gas handling system. While the vessel is equipped with three 1000W band heaters for heated experiments, the experiments described here were conducted at ambient temperature.

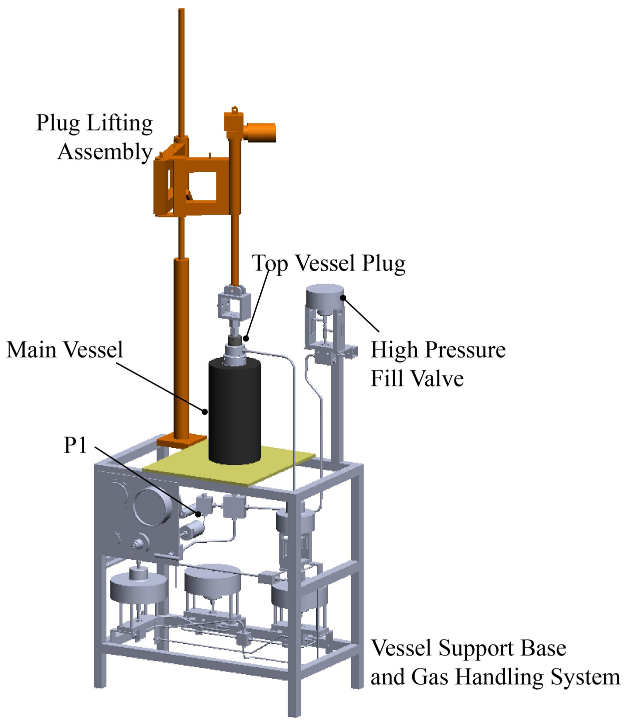

Figure 2. Illustration of hybrid closed bomb-strand burner facility.

The assembled strand was positioned within the strand support assembly and installed within the strand burner. The electrical connections to the ignitor and break wires were made. The reaction vessel was flushed with Argon. The flushing cycle starts with a ten second purge of nitrogen with a supply pressure of 500 psi at the regulator. After the nitrogen flow is stopped, the vessel is allowed to continue venting for an additional ten seconds. The flushing cycle is completed by the closing of the vent valve and the pressurizing of argon or helium to the regulated pressure that is applied to the two-stage booster pump. With the vessel sealed, the strand is ignited by applying a voltage across the Nichrome ignitor wire and the resulting pressure rise was recorded by three gauges. Two Kistler 4067A2000 (2000 Bar) gauges were flush mounted within the main vessel and a Kulite HEM-375-5000 (5000 psi) was located in the vent line approximately 20.3 cm (8 inches) downstream of the main vessel. In all tests, the pressures from the three gauges typically matched. Over the course of testing, combustion residue was found to get trapped within the vent line and the bottom of the reaction vessel. In one case, this residual material plugged the vent line such that the Kulite gauge recorded a lower pressure than the two Kistler gauges.

Time histories of the three pressure gauges, break wires, and ignitor current were recorded for each test. The voltage signal recorded from the break wires was recorded with 1 ms time resolution.

3 Experimental Results

The burn behavior of ten strands with initial densities between 58% and 88% TMD and initial pressures up to 2.0 MPa were investigated. Details of the tests are given in Table 2. The surface regression rates and the pressure histories within the vessel are presented in this section and individual plots of the measured data for each test are given in Appendix B.

Test ID	ϕ	P_0	P_{max}	Transition	
	(%)	(MPa)	(MPa)	χ	Π
3†	79.94	0.1515	2.193	–	–
5	79.94	0.1529	2.806	0.834	7.457
6	79.94	0.1812	2.737	0.834	5.468
7	79.94	2.0470	9.342	0.208	0.409
8	79.94	0.8224	4.391	0.417	0.637
9	88.29	0.1209	2.967	0.944*	14.335
10	67.84	0.1607	3.439	0.983	4.637
11	67.84	0.1941	2.981	0.983	4.858
12	88.29	1.0700	5.232	0.566	0.875
13	58.12	0.1403	1.508	0.287	1.023

Table 2. List of Strand Burner Tests. Vessel was filled with Argon. Break wires were recessed on the downstream side of pellets and a thick epoxy coating was used as a burn inhibitor on the strand perimeter. Parameters of χ and Π at transition refer to the effective bed volume ratio and vessel pressure ratio at the transition from conductive burn to deconsolidated burn within the porous bed as discussed in Section 3.2. † Unrecessed break wires in-between pellets and thin epoxy coating.

3.1 Vessel Pressure Histories

The vessel pressure histories for the experiments initially near ambient pressure are given in Figs. 3 and 4. All traces show the same general behavior including a time invariant baseline pressure, a pressure increase due to burning of the strand, and a post-burn plateau pressure. A more detailed look shows the small, yet rapid initial rise in pressure of approximately 0.15 MPa in all traces due to combustion of the black powder ignition increment. This initial pressure increase is followed by an increase of the vessel pressure in time during combustion of the pyrotechnic pellets. Small disturbances to this smooth pressure rise may be visible (such as in the 88% TMD strand and one of the 80% TMD strands) as a result of the pellet-to-pellet interfaces. There are two reasons for these disturbances. First, it is known that density gradients will exist in pellets of pressed powders such that a slightly higher density at the pressing ram face exists and this could cause slight variations in the combustion front velocity and vessel pressurization. The orientation of the pellets in each strand as related to the pellet face that was in contact with the pressing ram was not controlled. Second, the presence of the breakwires and trough cut into one face of the neighboring pellets may also cause this disturbance.

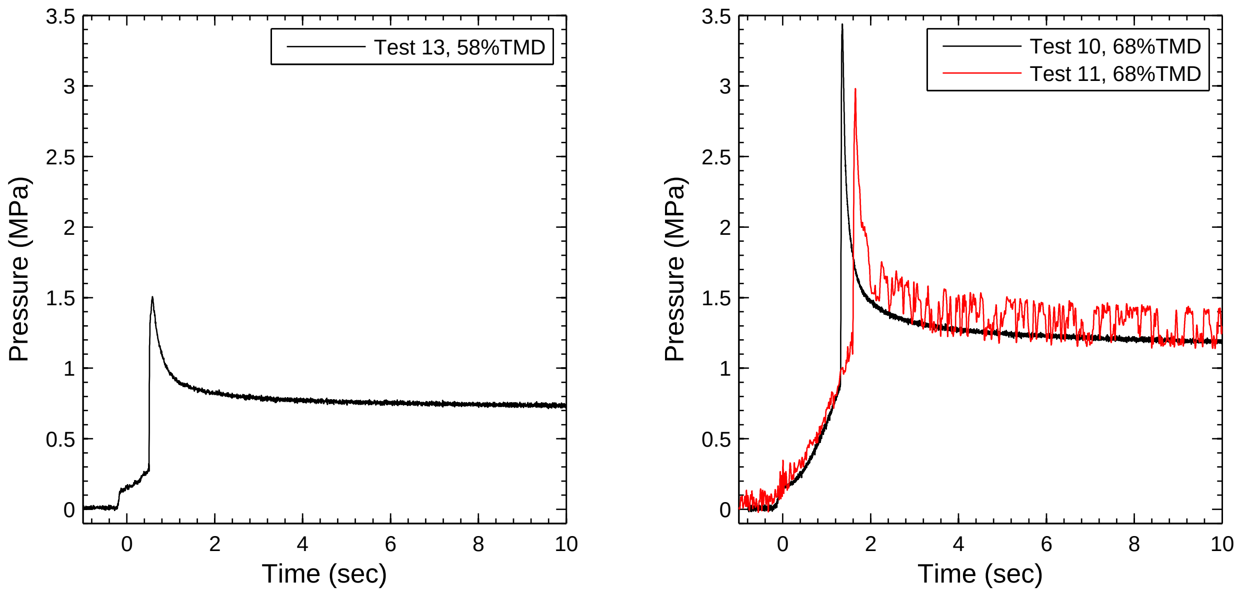

Figure 3. Comparison of the Vessel Pressure Histories for the 58% TMD strands (left) and 68% TMD strands (right).

In all tests, except for one of the 80% TMD tests, the vessel pressure discontinuously increased its rate of change after partially burning through the strand. As is shown in the next section, this discontinuous rise in pressure is also marked with a discontinuous increase in the surface regression rate indicating that transition to convective burning in the porous charge or also called "progressive deconsolidation" (Fifer and Cole, 1976) of the strand has occurred. Under these conditions, the surface regression rate is detemined by the particle parameters such as overall scale effects and burn rates associated with individual particles and localized groups of particles. After the vessel pressure reaches a maximum, the pressure decreases as heat transfer effects become evident and the product gases relax to equilibrium.

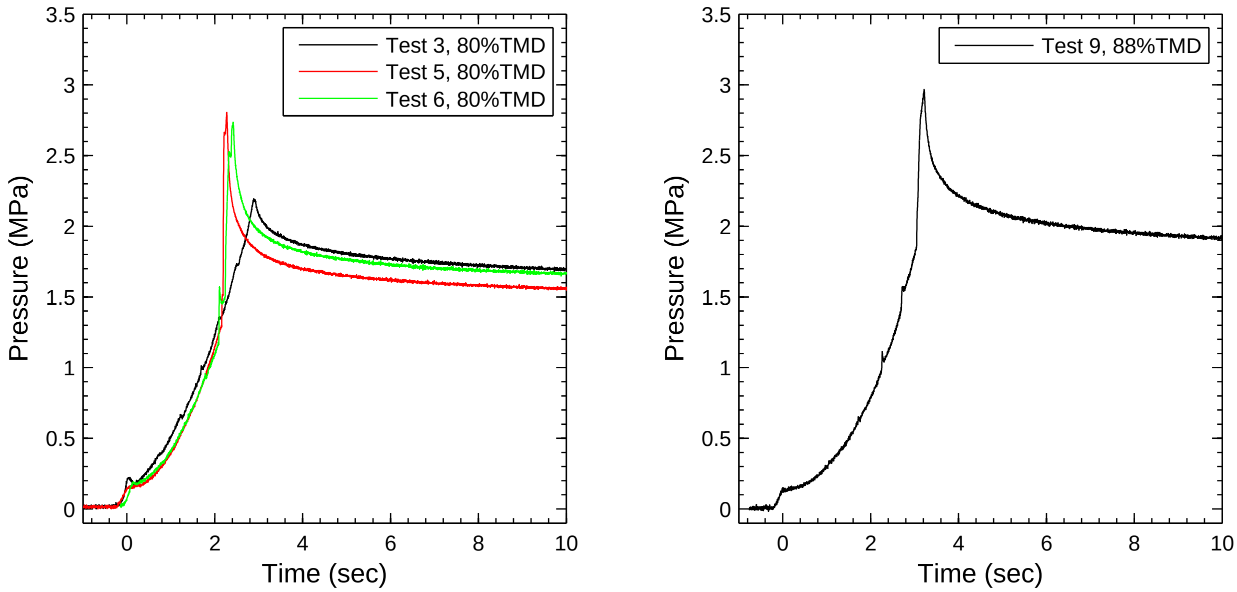

Figure 4. Comparison of the Vessel Pressure Histories for the 80% TMD strands (left) and 88% TMD strands (right).

3.2 Surface Regression Rates

A Matlab® program calculated the surface regression rate between successive break wires. The surface regression rate r is measured from the time between the electrical opening of successive break wires and their linear separation distance (equal to the pellet height).

$$r = (x_n - x_{n-1})/(t_n - t_{n-1}) \tag{1}$$

This regression rate is reported at the average pressure, $(P(t_n) + P(t_{n-1}))/2$. Figure 5 plots the burn rates for the tests of Table 2.

The logarithm of the surface regression rate increases linearly when plotted in terms of the logarithm of vessel pressure during the conductive portion of the burn. Upon transition to deconsolidated burning, the surface regression rate increases one or more orders of magnitude until the strand is consumed. Such transitions have been previously observed in the other THKP studies of Holy (1986), in the experiments of Tao *et al.* (1989) on two cast nitramine explosives, and the experiments of Maienschein *et al.* (2004) and Fifer and Cole (1976) on HMX-based explosives. Very notably, such transitions occur after an equivalently smaller fraction of the strand has been consumed in the zero-free-volume closed bomb experiments of Hingorani-Norenberg et al. (Hingorani-Norenberg and Moore, 1987; Hingorani-Norenberg *et al.*, 1990)

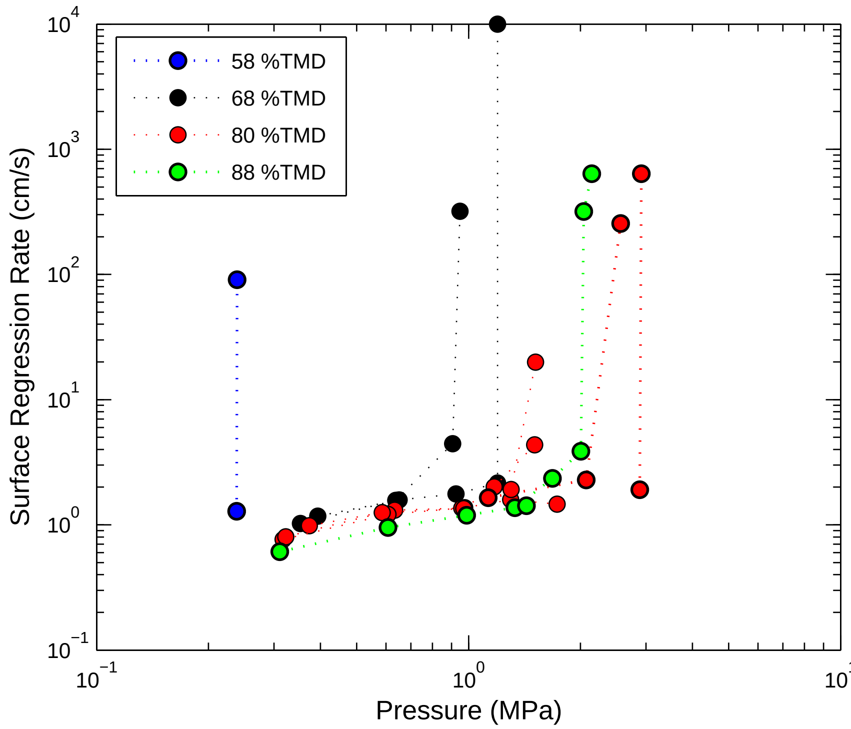

Figure 5. Plot of Measured Burn Rates versus Pressure for the tests listed in Table 2

A single test was conducted with a 58% TMD strand and transition to convective burning was noted within a single pellet. The data collected with 80% TMD and 88% TMD strands appear in Fig. 6. The data collected with 70% TMD strands is discussed in greater detail in the next section and is compared to the available data in the literature from Holy (1986).

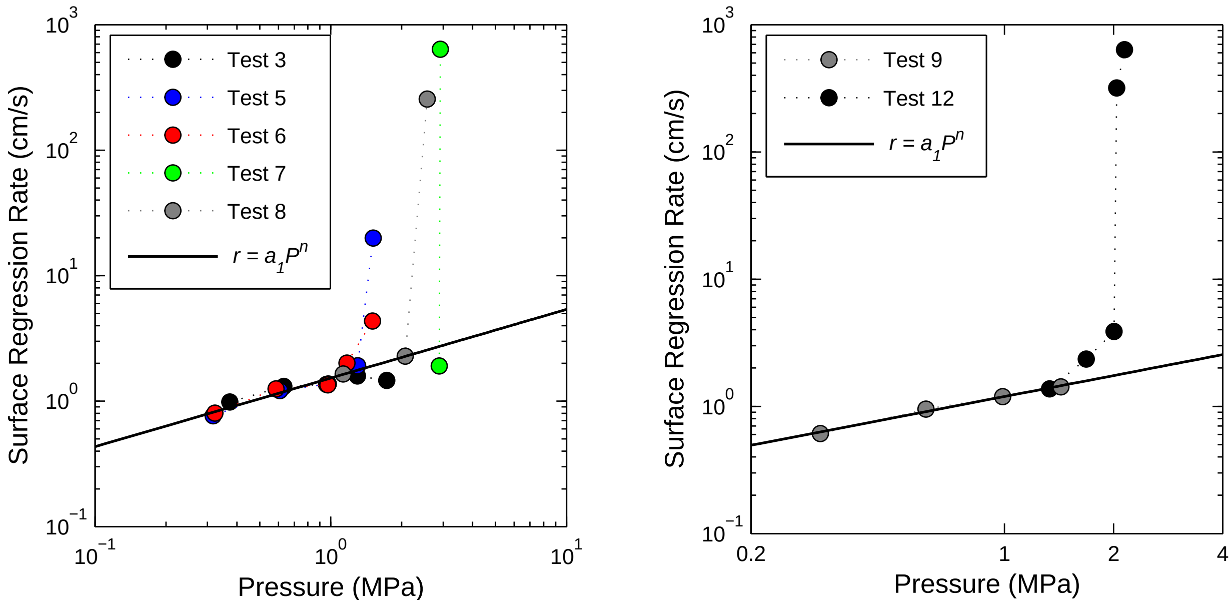

Figure 6. Plot of Measured Burn Rates versus Pressure for (left) 80% TMD Strands and Steady State Burn Rate Law ($a_1 = 1.5350$, $n = 0.5343$) and (right) 90% TMD Strands and Steady State Burn Rate Law ($a_1 = 1.1950$, $n = 0.5509$).

Conductive to convective burning is a large area of research for explosives based on the theories that increased pressurization allows for flame penetration into increasingly smaller cracks at increasingly higher flame velocities until the point of gaseous choked flow (Berghout *et al.*, 2002; Hill, 2005; Kondrikov and Karnov, 1992). In In porous beds that are pre-pressurized with an inert gas, as in the case our pyrotechnic strands and those of Holy (1986), the presence of the inert gas impedes the movement of the hot gases ahead of the combustion front that when combined with the increased burning rate at higher environment pressures (greater conversion of solid particles to gas) forces hot gases forward into the unburned powder bringing it to ignition faster. As noted in the experiments of Holy (1986) that only study the parameter of initial pressure, the transition to convective burning requires a startup process such that at higher initial vessel pressures, the transition occurs sooner in time from the onset of ignition.

The transition point where the discontinuous change in the rate of increase in vessel pressure (and measured surface regression rate) was tabulated in Table 2. Since this start-up process is related to the gas dynamic flow within the porous bed, there should be a correlation between the average initial bed density, the distance down the strand and the instantaneous vessel pressure when transition to deconsolidated burn occurs assuming that the amount of bed compaction preceeding the combustion front is negligible. Figure 7 shows the correlation between an effective bed volume ratio, χ

$$\chi = \frac{x}{L}\frac{\rho_c}{\rho} = \frac{x}{L}\frac{1}{(\mathrm{TMD})} \tag{2}$$

and the pressure ratio at transition.

$$\Pi = \frac{P - P_0}{P_0} \tag{3}$$

The data for the different initial density THKP strands and different initial pressures of this work are plotted along with three data points calculated from the published closed bomb pressure traces of Holy (1986). The data indicate a strong correlation between the effective bed volume ratio and pressure ratio at the point of transition further supporting the role that the bed permeability has in affecting the average surface regression rate of burning. The good correlation when using the initial average bed porosity indicates that under these hybrid closed-bomb strand burner conditions, significant bed compaction does not appear to affect this start-up process.

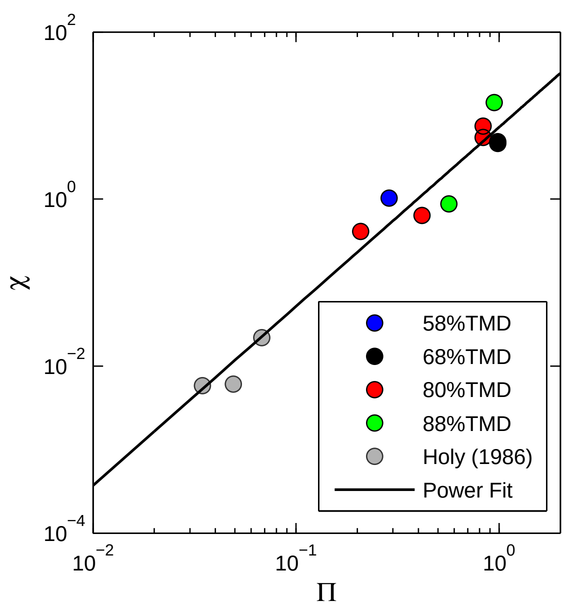

Figure 7. Correlation between effective porous bed volume ratio χ and vessel pressure ratio Π at the transition to deconsolidated burn within the pyrotechnic strand.

4 70% TMD Data and Literature Comparisons

Two tests were conducted with 70% TMD strands and a near-ambient pressure initial condition as shown in the surface regression rate data of Fig. 8 and the vessel pressure history data of Fig. 3. The black data points of Test 10 show steady burn with pressure until the onset of transition to deconsolidated burning. The data associated with the fourth break wire was not available. The grey data points of Test 11 show steady burn until an abrupt transition to deconsolidated burn. During the conductive burning regime, a fit of the surface regression data to the steady rate burn law resulted in the fitted parameters $a_1 = 1.9275$ and $n = 0.5558$ with an R^2 coefficient of 0.9692.

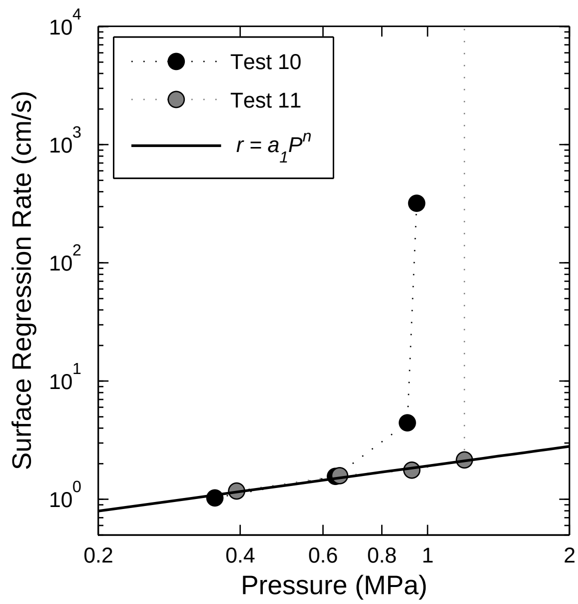

Figure 8. Plot of Measured Burn Rates versus Pressure for 70% TMD Strands and Steady State Burn Rate Law $r = 1.9275P^{0.5558}$.

The available literature for comparison consists of the experiments of Holy (1986). However, certain differences in the data collection and analysis as compared to this work should be noted. In the work of Holy (1986), a single-pellet strand is tested within a constant volume closed bomb vessel (initially containing either Helium or Nitrogen) such that the pressure history within the vessel is the only diagnostic. The beginning and ending times of the pellet burn are deduced from the recorded pressure history such that multiple experiments were conducted to establish the relationship of surface regression rate to pressure. A sample vessel pressure history given in Holy (1986) is reproduced in Fig. 9. The burn is considered to start when the pressure increases from the baseline value. During conductive burning, the pressure increases in a monotonic fashion. After approximate 4 ms, the pressurization rate of the vessel exceeds the linear pressurization rate until the burn is considered complete and the pressure is unchanged with time. This rise is pressure is similar to that observed in this work yet, differs likely due to the amount of material involved. Because a single-pellet strand is used, the amount of surface regression that occurred prior to the discontinuous rise in measured pressure must be inferred using the fitted value for the regression rate during the initial conductive burn. As a result, a linear surface regression is fit to the data masking the presence that transition to a different burning regime occurred. This linearly-assumed regression rate is assigned to the average vessel pressure during each test.

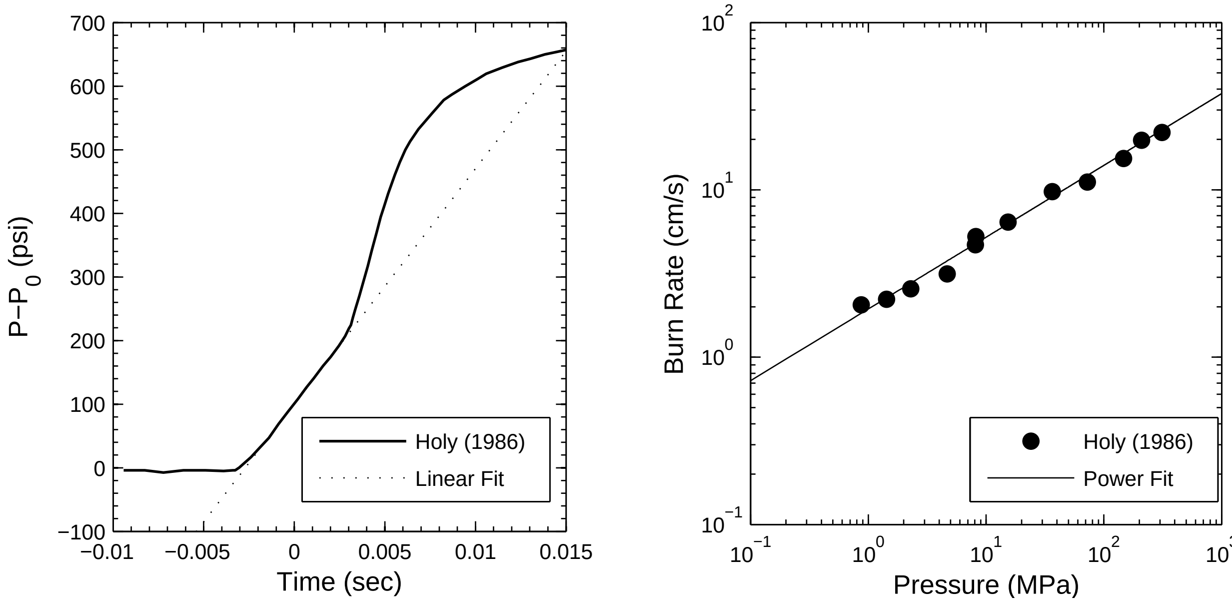

Figure 9. Representative Vessel Pressure History (left) and Burn Rate Plot (right) from Holy (1986). $r = a_1 P^n$ with $a_1 = 1.94$, $n = 0.429$.

The experimental data reported here for the 70% TMD strands are compared to the data of Holy (1986) in Fig. 10. It is important to note that the current data was collected in a vessel pressurized with Argon whereas Holy (1986) used Nitrogen and Helium. The different curve fits to the burn rate equation are given in Table 3.

Vessel Gas	a_1 (cm/s MPa^{-n})	n	Reference
He	2.41±0.29	0.384±0.025	(Holy, 1986)
N_2	1.94±0.15	0.429±0.015	(Holy, 1986)
Ar	1.9275	0.5558	Authors

Table 3. Table of Burn Rate Parameters a_1 and n

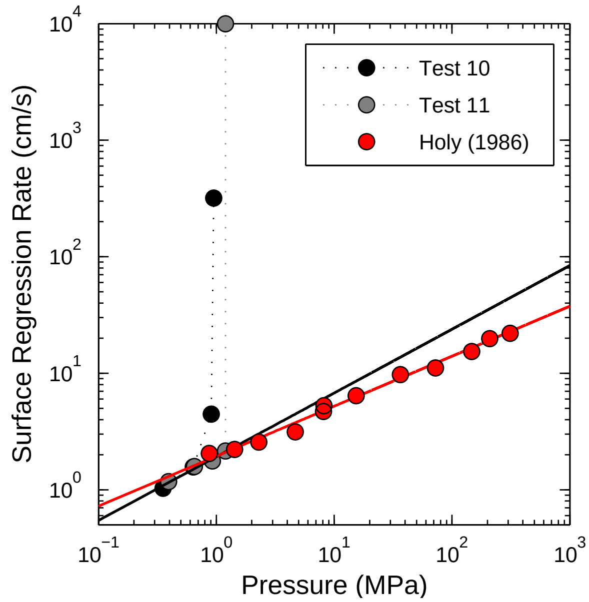

Figure 10. Comparison of 70% TMD data with Burn Rate Eqn ($a_1 = 1.9275$, $n = 0.5558$) from this work and data of Holy (1986) and $r = a_1 P^n$ with $a_1 = 1.94$, $n = 0.429$.

4.1 Closed Bomb Analysis Methods to Pyrotechnics

Closed bomb analysis has been able to represent the pressure-time behavior within a vessel during steady burning of propellants. The propellant community has followed two similar yet distinctly different paths in developing a mathematical formalism to predict the closed bomb pressure-time behavior. Namely, the experimental pressure-time history of the closed vessel can be used to predict the burning rate given assumptions about how the conversion from a solid sample with a known geometry to a volume of gas with a given amount of energy. This method originated with Juhasz and Price (1978), and refined by Glick and Haun (1990), and others. More recently, this approach was used by Yilmaz *et al.* (2008) where no assumptions are made as to the burning rate-pressure relationship yet the burning surface area is known and constant. An alternative method to analyzing closed bomb data follows that of Wiegand where heat transfer is ignored. Refinements to this formalism were carried out by Fayon and Goldstein (1966), and Celmins (1975). Shimpi and Krier (1975) developed methodology where the burning surface area is determined from geometric relationships relating to the web geometry of a propellant grain and a form of the burning rate-pressure relationship is assumed.

For application of these propellant-based closed bomb formalisms to our binder-less, porous-bed pyrotechnic strands, it is not expected that the burning surface regression would follow that of a propellant with defined geometric relationships, but rather on a more complicated relationship dependant on time-varying bed porosity, particle size, and gas permeability. Razani *et al.* (1990b), basically following the approach of Shimpi and Krier (1975), established a statistical representation of the burning surface area that depends on the particle sizes and size distributions. We proceed below with the simplier analysis assuming no heat losses and a constant burning surface to evaluate the collected closed vessel pressure histories.

Following the formulation Shimpi and Krier (1975), the major equations used to determine the time varying vessel pressure utilize the Noble-Abel equation for the burned gas mixture,

$$P(V_c - M_g \eta) = \frac{M_g R_0 T}{MW} \tag{4}$$

a steady state burning law

$$R = \frac{dx}{dt} = BP^n \tag{5}$$

where the force constant, λ is a function of the material

$$\lambda = \frac{R_0 T}{MW} \tag{6}$$

Considering the initial mass of material C and the fraction Z that has burned in time the the Nobel-Abel equation becomes

$$P - P_i = \frac{\lambda C Z}{V_c - C/\rho_s(1 - Z) - C\eta Z} \tag{7}$$

The complication comes into determining have$Z$ varies with time.

$$Z = 1 - \frac{V_s}{V_{0s}} \tag{8}$$

And assuming that geometry matters you can write a relationship for the remaining material at a giventime

$$dV_s = -S_x dx \tag{9}$$

The unknown parameter for a porous pyrotechnic bed is S_x. For the propellant community in which a burning grain with a known geometry is analyzed, all surfaces are assumed to receed uniformly such that the geometric relationships can be analytically derived or more approximately with the use of a form function as used in the Corner's or Hirschfelder's treatments. These relationships exist for slabs, cords, and single- and multi-perforated grains of propellants AMC (1964). Since S_x is not known a priori for a porous pyrotechnic bed, it is assumed to remain constant as suggested by the strong correlation between χ and Π at transition using the initial bed density (Fig. 7). If an infinitely thin combustion front is assumed, then the burn surface available at a given axial position within the bed would depend on the average void space between the pyrotechnic particles and the strand cross-sectional area.

$$\frac{S_x}{V_{0s}} = K\pi R^2 \phi \rho_c / C \tag{10}$$

where K is a fitting parameter to the measured data. It is known that the combustion front has a finite thickness and so K can be thought to represent the burn front thickness along the strand axis in terms of the initial bed porosity.

The remaining unknown is the covolume which is typically determined from a suitable equation of state. For zero-free-volume closed bomb analysis, a pressure- or density-dependant covolume relationship is necessary for accurate representation of the vessel pressure increase (Razani *et al.*, 1990b). For these experiments with a sufficiently large vessel, a constant, covolume approximation where $\eta \approx 1/\rho_s$ is assumed.

The predicted pressure histories during the conductive burn are plotted in Fig. 11 and Fig. 12 along with the measured vessel pressure histories. The predictions are shifted in time to begin at the first break wire signal. In general, the closed bomb approximated vessel pressure agreed with the experimentally recorded pressures for all densities. The highest density, 88% TMD, strand shows a greater difference in the rate of pressure rise between experiment and model likely due to the inaccuracies associated with the constant covolume approximation. Table 4 gives the values of the fitting parameter K required to alter the burning surface area at each strand density.

ϕ (%TMD)	K	S_x/V_{0s}
58.12±0.55	1.0	0.1914
67.84±0.28	1.5	0.1792
79.94±0.22	2.5	0.1661
88.29±0.51	4.5	0.1550

Table 4. Dependance of K on bulk strand density.

K is found to increase with increasing initial density however the product of K with the average void space based on the initial strand density is found to decrease with increasing initial density. This decrease in burning surface area with increasing strand density could be attributed to the lower permeability of the strand or the faster rate of surface regression. Novel experiments aimed at measuring this locally- and time-varying burning surface area in the porous pyrotechnic strands would be very interesting although very challenging. A more likely approach to determine a more realistic value of S_x/V_{0s} would be computational approaches that resolve the particles of the porous bed and can calculate the multiphase environment during propagation of the conductive burn front.

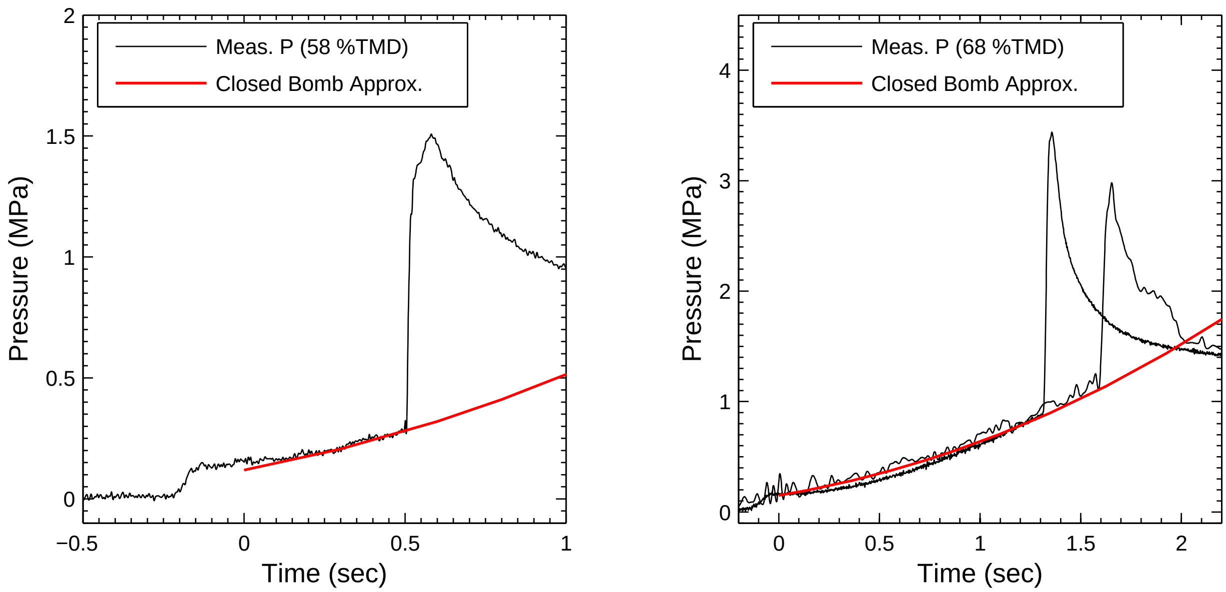

Figure 11. Measured vessel pressure histories with closed volume bomb analysis using covolume approximation for 60%TMD Strands (left) and 70%TMD Strands (right).

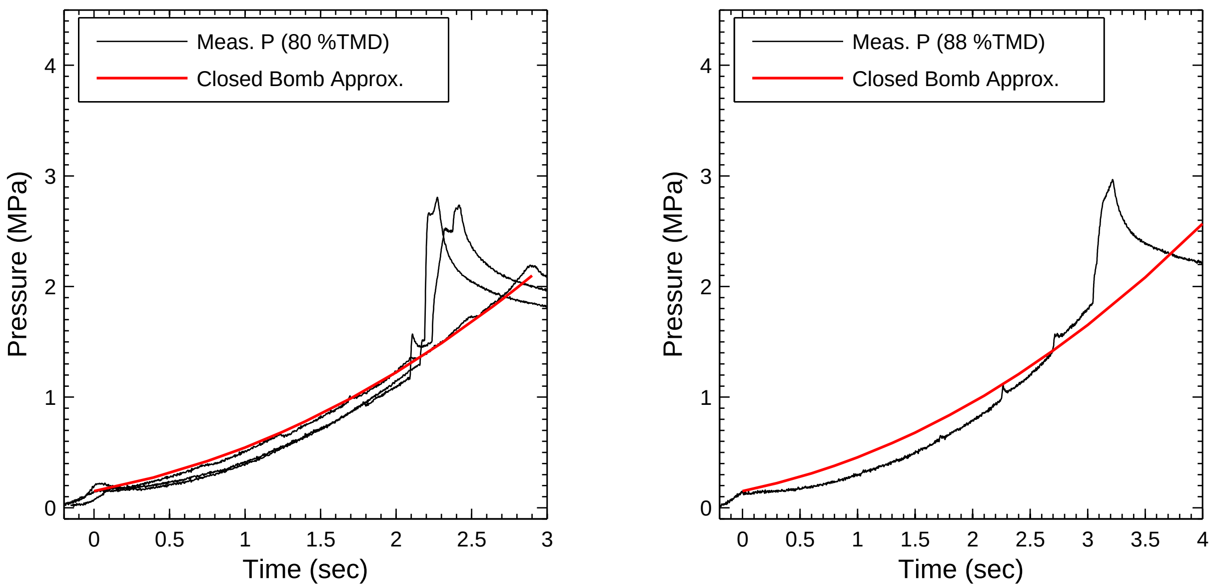

Figure 12. Measured vessel pressure histories with closed volume bomb analysis using covolume approximation for 80%TMD Strands (left) and 90%TMD Strands (right).

5 Conclusions

An experimental study was conducted to measure the burning behavior of THKP within a hybrid closed-bomb strandburner. This is the first presentation of this data as a function of strands varying initial average densities between 60-90% TMD and initial pressures between ambient and 100 MPa. Steady burn rates as a function of initial strand density were calculated. Evidence of transition from conductive to deconsolidated burning was presented and compared to the previous work of Holy (1986). A correlation between the effective bed volume ratio χ and the vessel pressure ratio Π at the transition to deconsolidated burn was presented suggesting that for these conditions there is no significant changes to the average bed density (such as compaction or fragmentation) during the conductive burn regime. After this transition, the burn is highly erratic with sruface regression rates orders of magnitude greater than the conductive regression rates or in some cases, the apparant complete loss of the remaining strand segments or complete deconsolidation of the porous pellets. An analogy to the closed bomb analysis methods commonly used with propellants is made to predict the vessel pressure rise during the conductive burning regime assuming that the burning surface area remains constant and related to the average initial bed porosity arocss the strand cross-section.

References

(1964). *Engineering Design Handbook - Ammunition Series, Section 4, Design For Projection*. U.S. Army Materiel Command, AMCP AM 706-247.

Baer, M. R. and Shepherd, J. E. (1983). A thin flame model for reactive flow in porous materials. Technical report, Sandia National Laboratories. SAND83-2576.

Beck, M. W. and Brown, M. E. (1986). Burning of antimony/potassium permanganate pyrotechnic compositions in closed systems. *Combustion and Flame*, **65**, 263–271.

Begeal, D. R. and Stanton, P. L. (1982). Pyrotechnic deflagration velocity as a function of permeability. In *Proceedings of the 8th International Pyrotechnics Seminar*.

Berghout, H. L., Son, S. F., Skidmore, C. B., Idar, D. J., and Asay, B. W. (2002). Combustion of damaged pbx 9501 explosive. *Thermochimica Acta*, **384**, 261–277.

Celmins, A. (1975). Solid propellant burning rate measurements in a closed bomb. BRL-1840, U.S. Army Ballistic Research Laboratory.

Collins, L. W., Haws, L. D., and Gibson, A. (1980). The electrostatic initiation of nondispersed pyrotechnics. *Combustion and Flame*, **38**, 155–158.

Erickson, K. L. (1984). Effect of oxide coating thickness of thermal ignition of titanium-based pyrotechnics. In *International Pyrotechnics Seminar*. SAND84-0459C.

Erickson, K. L., Rogers, Jr., J. W., and Ward, S. J. (1986). Titanium oxidation kinetics and the mechanism for thermal ignition of titanium-based pyrotechnics. In *Proceedings of the 11th International Pyrotechnics Seminar*.

Erickson, K. L., Rogers, Jr., J. W., and Skocypec, R. D. (1987). Thermal ignition of Ti-based pyrotechnics II: Oxidation kinetics applied to analysis of slow ignition (DTA) experiments. In *Proceedings of 12th International Pyrotechnics Seminar*.

Erickson, K. L., Skocypec, R. D., Rogers, Jr., J. W., and Massis, T. M. (1989). Powder morphology effects in the ignition of titanium-based pyrotechnics. In *Proceedings of 14th International Pyrotechnics Seminar*. SAND89-0344C.

Fayon, A. M. and Goldstein, J. B. (1966). Evaluation of solid propellant ballistic properties by constant volume burning. *Combustion and Flame*, **10**, 23–28.

Fifer, R. and Cole, J. (1976). Transitions from laminar burning for porous crystalline explosives. In *Seventh Symposium (International) on Detonation*, Annapolis, MD.

Glick, R. L. and Haun, D. V. (1990). An improved closed burner method. AIAA90-1870.

Hill, L. G. (2005). Burning crack networks and combustion bootstrapping in cookoff explosions. In *Shock Compression of Condensed Matter*. American Physical Society. Shock Compression of Condensed Matter.

Hingorani-Norenberg, S. L. and Moore, L. M. (1987). Preliminary burn rate studies on TiH1.65/KClO4. Technical report, Sandia National Laboratories. SAND87-3029C.

Hingorani-Norenberg, S. L., Razani, A., and Shahinpoor, M. (1990). Compaction of TiH1.65/KClO4 pyrotechnic powder during confined burn. Technical Report SAND90-0600C, Sandia National Laboratories.

Holy, J. A. (1986). Pressure dependent burn rates of TiHx/KClO4 (x = 0.2, 0.65, 1.65). In *Proceedings of the 11th International Pyrotechnics Seminar*.

Holy, J. A. (1993). Burn rates of TiH2/KClO4/viton and output testing of NASA SKD26100098-301 pressure cartridges. Technical report, National Aeronautics and Space Administration. NASA Contractor Report 188357.

Juhasz, A. A. and Price, C. F. (1978). The closed bomb technique for burning rate measurement at high pressure. In T. L. Boggs and B. T. Zinn, editors, *Experimental Diagnostics in Combustion of Solids*, volume 63 of *Progress In Astronautics and Aeronautics*, New York. American Institute of Aeronautics and Astronautics.

Kondrikov, B. N. and Karnov, A. S. (1992). Transition from combustion to detonation in charges with a longitudinal cylindrical channel. *Combustion, Explosion, and Shock Waves*, **28**, 263–269.

Kosanke, K., Kosanke, B. J., von Maltitz, I., Sturman, B., Shimizu, T., Wilson, M. A., Kubota, N., Jennings-White, C., and Chapman, D. (2004). *Pyrotechnic Chemistry: Pyrotechnic Reference Series, No. 4*. Journal of Pyrotechnics, Inc.

Maienschein, J. L. and Chandler, J. B. (1998). Burn rates of pristine and degraded explosives at elevated pressures and temperatures. In *Eleventh Symposium (International) of Detonation*. International Detonation Symposium. Snowmass Village, CO.

Maienschein, J. L., Wardell, J. F., DeHaven, M. R., and Black, C. K. (2004). Deflagration of HMX-based explosives at high temperatures and pressures. *Propellants, Explosives, Pyrotechnics*, **29**(5), pp. 287–295.

Massis, T. M. (1996). The processing, properties, and use of the pyrotechnic mixture titanium subhydride/potassium perchlorate. AIAA 32nd Joint Propulsion Conference and Exhibit, Lake Buena Vista, FL.

Massis, T. M., Morenus, P. K., and Merrill, R. M. (1975). Stability of the pyrotechnic mixture titanium hydride (TiHx)/potassium perchlorate (KClO4). Technical Report SAND75-7889, Sandia National Laboratories, Albuquerque, New Mexico, USA.

Price, C. and Juhasz, A. (1977). A versatile user-oriented closed bomb data reduction program (cbred). BRL Report No. 2018.

Rajendran, A., Kartha, C., and Babu, V. (2000). Burn rate studies of a titanium-based pyrotechnic smoke composition. *Defence Science Journal*, **50**(2), 199–206.

Razani, A. and Shahinpoor, M. (1988). Transient burning analysis of pyrotechnic materials in a closed bomb. In *Proceedings of the Thirteenth International Pyrotechnics Seminar*, pages pp. 931–947. SAND88-7097C.

Razani, A., Shahinpoor, M., and Hingorani-Norenberg, S. L. (1990a). Effect of equations of state on transient burning analysis of pyrotechnic materials in a closed system. In *32nd Annual Meeting, Pyrotechnics and Explosives Applications Section, ADPA*. SAND90-1851C.

Razani, A., Shahinpoor, M., and Hingorani-Norenberg, S. L. (1990b). Semi-analytical model for pressure-time history and granular pyrotechnic materials in a closed system. In *Proceedings of the Fifteenth International Pyrotechnics Seminar*. SAND90-0599C.

Rogers, Jr., J. W., Erickson, K. L., Belton, D. N., Springer, R. W., Taylor, T. N., and Berry, J. G. (1988-89). Low temperature diffusion of oxygen in titanium and titanium oxide films. *Applied Surface Science*, **35**, 137–152.

Shimpi, S. A. and Krier, H. (1975). The closed bomb test for the assessment of solid propellant grains utilized in guns. *Combustion and Flame*, **25**, 229–240.

Sorensen, D. N., Quebral, A. P., Baroody, E. E., and Sanborn, W. B. (2006). Investigation of the thermal degradation of the aged pyrotechnic titanium hydride/potassium perchlorate. *Journal of Thermal Analysis and Calorimetry*, **85**, 151–156.

Tao, W. C., Costantino, M. S., and Ornellas, D. L. (1989). Burning rates of two cast nitramine explosives using a hydbrid closed bomb-strand burner. In *Ninth Symposium (International) on Detonation*. Portland, OR.

Velicky, R. W. (1983). The burning behavior of TNT in the closed bomb. *Journal of Energetic Materials*, **1:2**, 177–205.

Yilmaz, N., Donaldson, B., Gill, W., and Erickson, W. (2008). Solid propellant burning rate from strand burner pressure measurement. *Propellants, Explosives, Pyrotechnics*, **33**, 109–117.

6 Appendix A

Test ID	Break Wire Number	Pressure (MPa)	Surface Regression Rate (cm/s)
3	1	0.1515	0
	2	0.3731	0.9847
	3	0.6331	1.3083
	4	0.9589	1.3600
	5	1.2980	1.5868
	6	1.7290	1.4630
5	1	0.1529	0
	2	0.3174	0.7649
	3	0.6077	1.2113
	4	0.9765	1.3702
	5	1.3009	1.9190
	6	1.5149	19.9118
6	1	0.1812	0
	2	0.3228	0.8032
	3	0.5859	1.2523
	4	0.9712	1.3478
	5	1.1725	2.0131
	6	1.5056	4.3575

Table 5. Surface regression rate data for Tests 3, 5, and 6.

Test ID	Break Wire Number	Pressure (MPa)	Surface Regression Rate (cm/s)
7	1	2.0470	0
	2	2.8851	1.9048
	3	2.9156	636.778
8	1	0.8224	0
	2	1.1294	1.6463
	3	2.0705	2.2795
	4	2.5650	255.2216
9	1	0.1209	0
	2	0.3107	0.6110
	3	0.6071	0.9507
	4	0.9884	1.1931
	5	1.4314	1.4222
10	1	0.1607	0
	2	0.3533	1.0269
	3	0.6374	1.5669
	5	0.9058	4.4487
	6	0.9486	319.1870
11	1	0.1941	0
	2	0.3930	1.1737
	3	0.6507	1.5825
	4	0.9256	1.7634
	5	1.1971	2.1547
	6	1.1971	inf
12	1	1.0700	0
	2	1.3324	1.3691
	3	1.6805	2.3536
	4	2.0056	3.8700
	5	2.0418	318.3890
	6	2.1449	636.7780
13	1	0.1403	0
	2	0.2381	1.2835
	3	0.2388	90.9034

Table 6. Surface regression rate data for Tests 7-13.

7 Appendix B

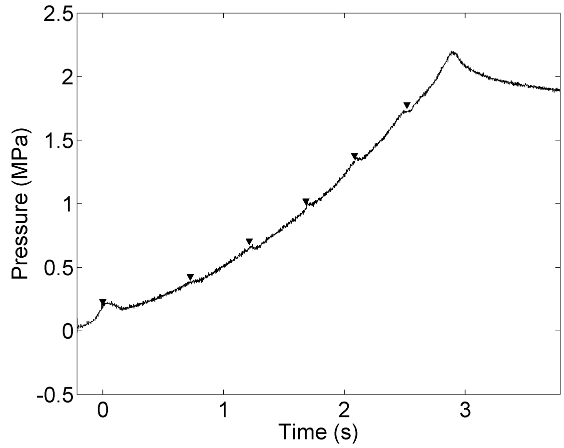

Figure 13. Pressure and break wire output from test 03

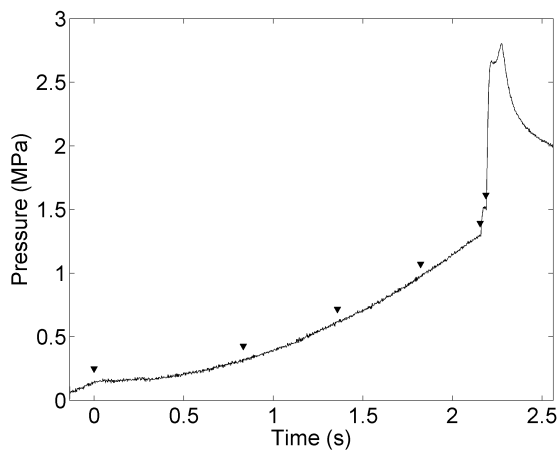

Figure 14. Pressure and break wire output from test 05

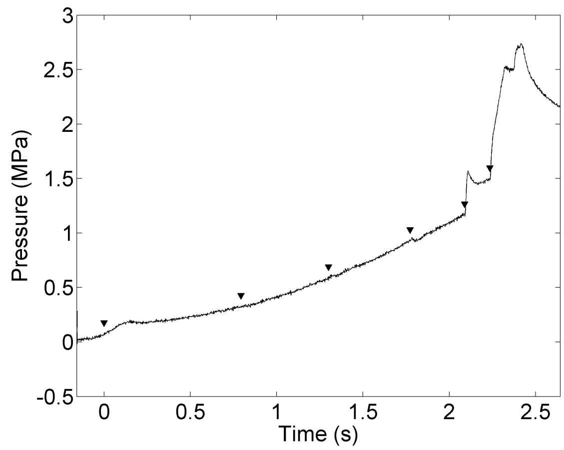

Figure 15. Pressure and break wire output from test 06

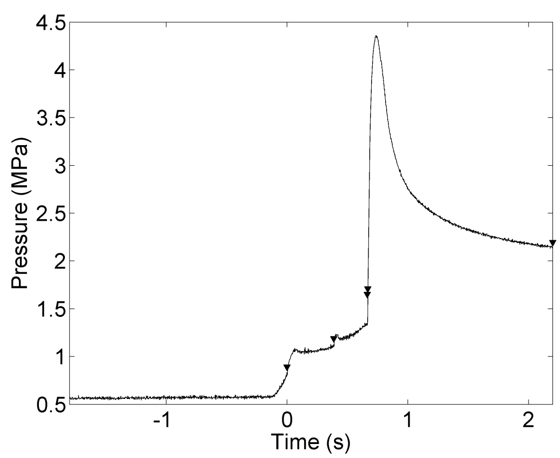

Figure 16. Pressure and break wire output from test 08

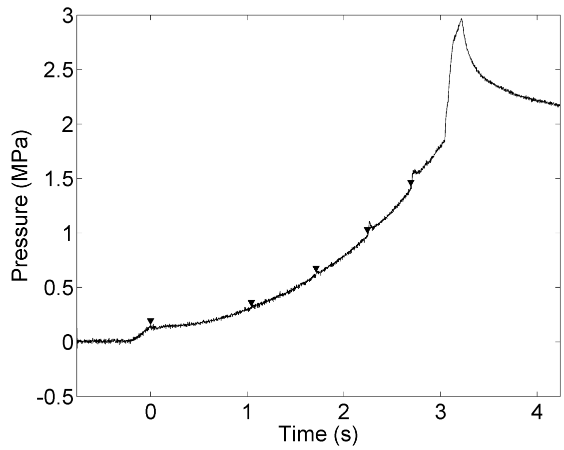

Figure 17. Pressure and break wire output from test 09

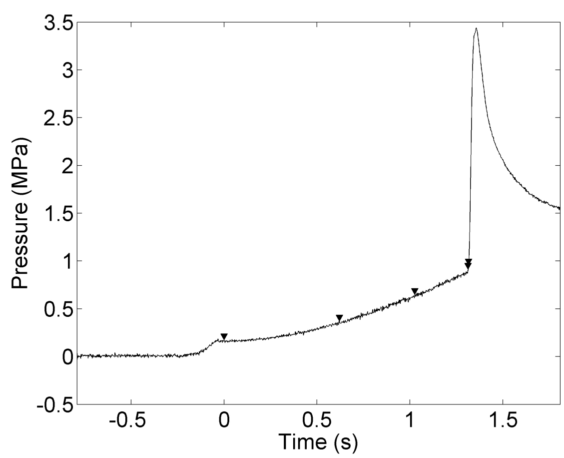

Figure 18. Pressure and break wire output from test 10

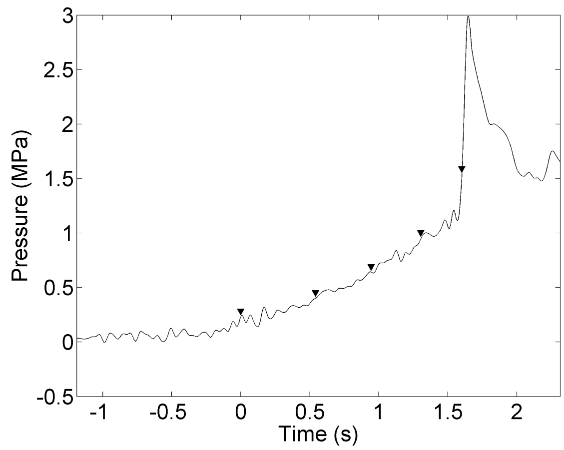

Figure 19. Pressure and break wire output from test 11

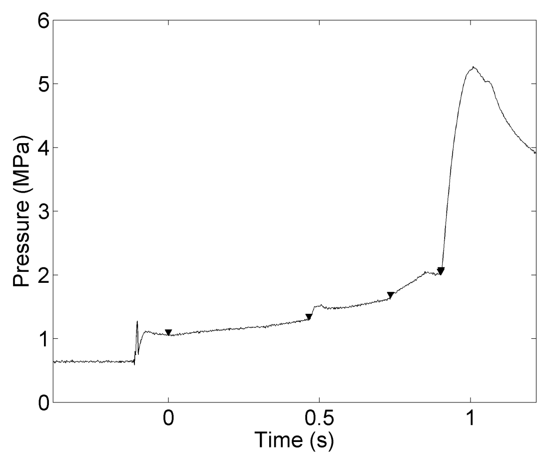

Figure 20. Pressure and break wire output from test 12

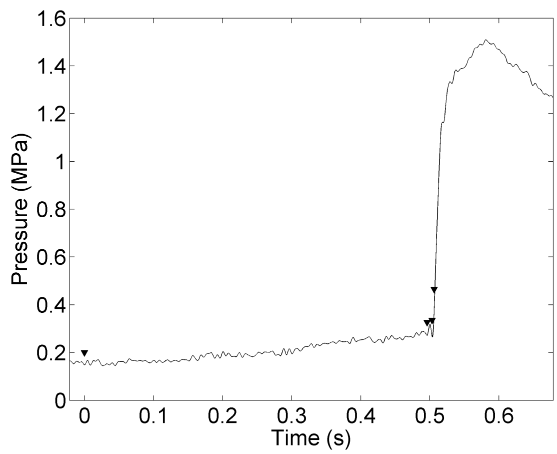

Figure 21. Pressure and break wire output from test 13

DISTRIBUTION:

1	MS 0836	W. Erikson, 01516
1	MS 0836	A.S. Geller, 01513
1	MS 0836	M. Hobbs, 01516
1	MS 0836	C.D. Yarrington, 01516
1	MS 1452	D. Damm, 02554
1	MS 1452	E.S. Hafenrichter, 02552
1	MS 1452	T.L. Hendricks, 02552
1	MS 1452	M.K. Knowles, 02552
1	MS 1452	R.T. Marinis, 02554
1	MS 1452	G.A. Radtke, 02552
1	MS 1453	J.L. Moya, 02550
1	MS 1454	M.J. Kaneshige, 02554
1	MS 1455	L.M.G. Minier, 02554
1	MS 9056	J.J Kay, 08128
1	MS 9056	S.P. Maharrey, 08128
1	MS 0899	Technical Library, 9536 (electronic copy)

Sandia National Laboratories